Investigations in the fabrication of surface patterns for wettability modification on a Zr-based bulk metallic glass by nanosecond laser surface texturing

Yang Jiao[1], Emmanuel Brousseau[1*], Xiaojun Shen[2], Xiaoxiang Wang[3], Quanquan Han[1], Hanxing Zhu[1], Samuel Bigot[1], Weifeng He[4]

1. Cardiff School of Engineering, Cardiff University, Cardiff, CF24 3AA, United Kingdom

2. School of Mechanical, Aerospace and Automotive Engineering, Coventry University, Coventry, CV1 5FB, United Kingdom

3. Institute of Industrial Ecology and Environment, College of Chemical and Biological Engineering, Zhejiang University, Hangzhou, 310027, China

4. Institute of Aeronautics Engine, School of Mechanical Engineering, Xi'an Jiaotong University, Xi'an, Shaanxi, 710049, China

Abstract: Laser texturing has previously been employed to enhance the wettability of metallic alloys. Such studies reported that modifying the wettability of a surface is a result of changes in both its topography and its chemistry. In this paper, an investigation about laser-induced surface wettability modification is also reported but for a less studied type of material in this context. In particular, nanosecond (ns) laser processing was employed to texture two types of surface patterns, i.e. dimples and grooves, on the surface of a Zr-based bulk metallic glass (BMG) known as Vitreloy 105. The specific focus of the research was on understanding the role played by both surface topography and chemistry modifications in changing the wettability of the original surface. Using static contact angle measurements, it was found that groove patterns enhanced the hydrophilicity of the original BMG, while dimple patterns weakened it. Based on the obtained 3D surface measurements and XPS data, it is suggested that the reduced hydrophilicity of dimple-textured surfaces was driven by the decrease of hydrophilic C=O and O=C-O bonds post laser processing. While these bonds were also reduced for groove-textured patterns, the hydrophilicity was still enhanced following laser irradiation as a result of the dominant role that a much larger induced surface roughness should play in this case.

Keywords: Nanosecond laser surface texturing; Bulk metallic glass; Wettability; Surface topography; Surface chemistry.

1. Introduction

Since being first discovered in the early 1990s, BMGs in metal-metal systems have received sustained attention from the research community during the past few decades as a result of their combined desirable physical and mechanical properties (Liaw and Miller, 2008). This include their generally high yield strength (Löffler, 2003), relatively low Young's modulus (Bian et al., 2001), high hardness (Telford, 2004), good wear and corrosion resistance (Huang and Yan, 2017a) as well as high elastic limit (Li and Zheng, 2016). Among the different domains envisaged by the research community, where such alloys may be employed, the sector concerned with biomedical applications has been proposed as potentially relevant (Li and Zheng, 2016). However, when considering BMGs as potential biomaterials, improving their bio-compatibility with tissues is a key factor since the reaction of implants with the host tissue determines their long-term performance. As reported by a number of researchers such as Ponsonnet et al. (2003) for instance, bio-compatibility depends on surface wettability to a great extent. In particular, a higher wettability, i.e. enhanced hydrophilicity, has beneficial influence on the cell/protein attachment, growth, proliferation and differentiation. In this context, the development of engineering techniques to increase the hydrophilicity of BMG surfaces constitute an important research topic.

Among existing surface modification methods, laser texturing represents an environmentally-friendly and relatively fast technique that relies on short (nanosecond) or ultra-short (picosecond or femtosecond) laser pulses to fabricate a wide range of nano- and micro-scale structures. With regards to altering the wettability of an original surface, several types of structures fabricated by laser texturing have already been reported on metallic substrates. In the case of orthopaedic titanium alloys for

instance, researchers have observed a wide range of surface wettability modifications, from super-hydrophilic to super-hydrophobic depending on the fabricated surface patterns and the laser parameters utilised. For example, Pfleging et al. (2015) successfully improved the surface hydrophilicity of Ti-6Al-4V via the texturing of two kinds of surface patterns, i.e. dimples and grooves, using a nanosecond ArF excimer laser. The obtained groove-textured surface showed better hydrophilicity than that of the dimple-textured surface. These authors attributed this result to the larger surface area induced by the groove patterns. This research group further investigated the bio-compatibility of the same titanium alloy with these two surface structures in a study from Kumari et al. (2015). In this case, it was shown that laser texturing could increase the bio-activity of the alloy in Hank's solution and that no cytotoxic substances were produced. It was also found that the groove-textured surface resulted in a better cell attachment compared to the as-cast and dimple-textured surfaces. Furthermore, the cell attachment results showed good correlation with the corresponding wettability measurements, which further supports the positive effect that enhanced hydrophilicity has on cell behaviour. In another study, Li et al. (2016) managed to produce stable super-hydrophilic, hydrophilic, hydrophobic and super-hydrophobic surfaces on a titanium alloy via laser texturing coupled with the silanization process. In particular, the textured surfaces could be tuned to be hydrophilic or super-hydrophilic and subsequently became hydrophobic or super-hydrophobic after silanization. The super-hydrophilic to super-hydrophobic transition was attributed to the reduced content of surface hydroxyl groups introduced by the silanization treatment. This study added to the body of literature on the influence of surface chemical groups on the wettability of a surface. In fact, the literature indicates that laser-induced changes in the carbon content and type on metallic substrates should be an important contributor to the evolution of wettability following laser processing. Kietzig et al. (2009) proposed that an increase in the presence of non-polar carbon species on the surface of different metallic alloys led to weakened hydrophilicity and switch to hydrophobic behaviour in the days following femtosecond laser irradiation. Bizi-Bandoki et al. (2013) studied the evolution over time of the wettability of two metallic substrates (i.e. aluminium alloys and stainless steel) patterned with periodic structures using femtosecond laser texturing. These authors observed that the wettability modification of a processed surface depended not only on the laser-induced changes in topography and but also in subsequent variation of the surface chemistry. For instance, in the case of the aluminium specimens, the hydrophobic behaviour reached after 2 to 3 days was explained by the presence of new non-polar carbon groups. More recently, Huerta-Murillo et al. (2019) studied the effect of storage conditions on changes in the chemical composition and wettability of Ti-6Al-4V laser-patterned surfaces. In particular, when assessing the different carbon bonds present, these authors observed that surfaces with reduced polar molecules, i.e. carbon-oxygen (C-O) and carbonyl bonds (C=O) and O=C-O species, were also associated with hydrophobic behaviour.

In the specific field of laser texturing of BMG materials, the literature is still scarce regarding efforts to tune the wettability of such surfaces. The study by Huang and Yan (2017b) is the only report investigating the effect of laser surface texturing on the wettability of a BMG substrate. In this particular study, the BMG commonly known as Vitreloy 1 was investigated. However, Vitreloy 1 cannot be considered as a suitable biomaterial since it contains the toxic element beryllium. Besides, the reported laser processing operations resulted in increased hydrophobicity, which is not a desired outcome for potential orthopaedic implant applications. In addition, the wettability modification was only discussed in relation to laser-induced topographical changes. However, as reported above, it is expected that the tuning of the wettability of a surface should depend on both the alteration of its topography and also its chemistry. Therefore, further research efforts aimed at modifying the wettability of BMGs and also, focussed on understanding the associated driving mechanisms, are important to promote such amorphous alloys in bio-applications. Among all the metal-metal systems, Zr-based BMGs have been widely investigated given that 1) they generally have good glass forming ability making the synthesis of large-size component possible (Li and Zheng, 2016); 2) a number of compositions have been made commercially available since their discovery (Telford, 2004) and 3) Zr is considered as a biocompatible element (Huang et al., 2011).

In this context, a nanosecond fibre laser was utilised in this study to fabricate two types of surface structures, i.e. dimple and groove patterns, on a Vitreloy 105 Zr-based BMG. While not containing the toxic element beryllium and in addition to the generic attractive characteristics of this alloy, commonly

shared with BMGs in terms of mechanical and chemical properties, (Naleway et al., 2013) also reported its excellent fatigue performance. An important aspect of this study is that both the surface topography and chemistry of the laser textured surfaces was investigated to evaluate their respective role in the laser-induced modification of surface wettability.

2. Materials and methods

2.1. Specimens preparation

The Zr-based BMG Vitreloy 105 with nominal composition $Zr_{52.8}Cu_{17.6}Ni_{14.8}Al_{9.9}Ti_{4.9}$ (at.%) (purchased from Visser Precision, Denver, USA) was chosen for this investigation due to its excellent fatigue properties. It can be noted that the composition of the produced alloy was very slightly different from the standard composition of Vitreloy 105, which is $Zr_{52.5}Cu_{17.9}Ni_{14.6}Al_{10}Ti_5$. The as-received master ingots with dimensions of 3 mm in diameter and 10 mm in length were first cut into disks with a thickness of 3 mm using wire electrical discharge machining (EDM). All disk samples were then mounted in conductive resin with the top surface left exposed for subsequent processing. Although the energy used during the wire EDM cut was as low as possible, the cutting process may still have resulted in the generation of a layer containing crystalline precipitates in addition to the formation of a relatively rough surface. Hence, before laser irradiation, the exposed surface of each sample was mechanical ground using consecutively 1200 and 2000 grid SiC papers. Next, these were further polished to a mirror-like appearance with a 1 µm diamond gel suspension before being ultrasonically cleaned with acetone for at least 15 minutes to remove debris and small particles.

2.2. Nanosecond laser surface texturing

Nanosecond laser processing operations were conducted on the Vitreloy 105 specimen surfaces using a 20 W pulsed Yb-doped fibre laser system (from SPI Lasers, UK). This system produced a near-Gaussian (M^2<2) laser beam with a wavelength of 1064 nm. The laser beam was focused by a 100 mm focal lens with an incident angle perpendicular to the surface of the samples. This resulted in an effective spot diameter of 32 µm. This value was used to assess the delivered fluence. In a previous study from the current authors, (Jiao et al., 2019) investigated the effect of pulse duration on the surface topography and observed that longer pulses could remove a larger volume of material in a given time period. Therefore, the maximum available pulse duration, i.e. 220 ns, was chosen. The average fluence, F, ranged from 10 to 50 J/cm^2. Two kinds of structures, i.e. dimples and grooves, were fabricated on the surface of the specimens via programming the motion of a computer-controlled three-axis platform. The scanning speed values considered, v, ranged between 100 and 300 mm/s. The lateral distance, A, between two consecutive laser pulses was determined and controlled via the scanning speed as follows:

$$A = v/f \tag{1}$$

The longitudinal displacement, d_s, was directly set by the machine parameter “track distance” and ranged from 60 to 110 µm. Compared to the spot diameter of 32 µm, this interval was large enough to avoid the overlapping of two neighbouring lines of laser irradiation. A schematic of the laser texturing for these two types of structures is shown in Fig. 1. In the case of the dimple structures, the values of d_s and A were set to be equal. All operations were conducted in ambient atmosphere. The parameters fluence, F, scanning speed, v, and track distance, d_s, were varied in order to explore their influence on the wettability of the Vitreloy 105 surfaces. Areas of 2 × 2 mm were patterned with different laser parameters and scanning strategies, which are summarised in Table 1.

Table 1
Laser parameters employed for the fabrication of dimple and groove patterns on the surface of Vitreloy 105 samples.

Wavelength (nm)	Spot diameter (μm)	Pulse duration (ns)	Frequency (kHz)	Laser fluence (J/cm²)	Scanning speed (mm/s)	Track distance (μm)	Surface patterns
1064	32	220	20	10	-	80	Dimples
				30	-	80	
				50	-	80	
				30	-	60	
				30	-	70	
				30	-	90	
				30	100	100	Grooves
				30	200	100	
				30	300	100	
				30	200	80	
				30	200	90	
				30	200	110	

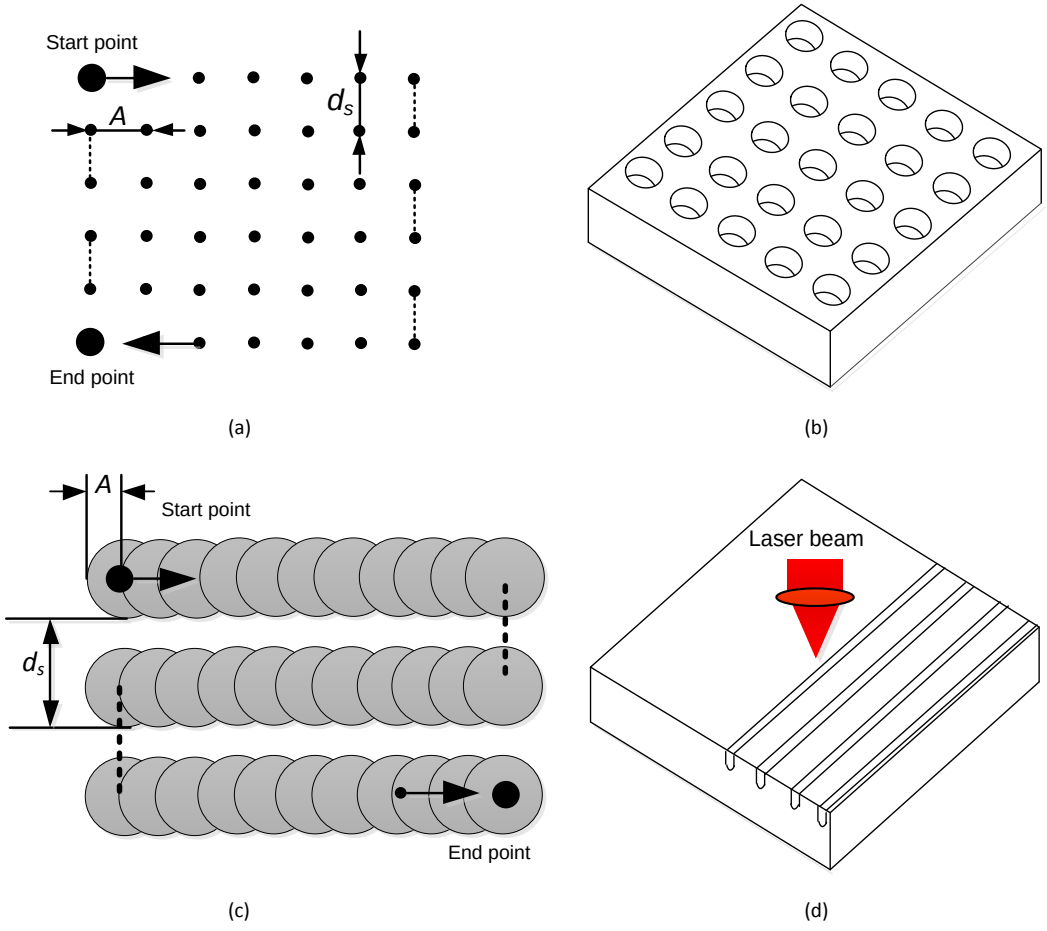

Fig. 1. Schematic diagram of laser scanning strategies for the fabrication of dimple and groove patterns on the Vitreloy 105 surfaces; (a) and (c) are the top view of the laser path for dimples and grooves, respectively; (b) and (d) illustrate the respective patterns on the laser-textured surfaces.

2.3. Analysis of wettability

Contact angle measurements are commonly used to quantify the wettability of a solid surface. These are described by the Young-Dupre's equation:

$$\gamma_S = \gamma_{SL} + \gamma_L \cos\theta_c \tag{2}$$

where θ_c is the equilibrium contact angle, γ_S is the surface free energy of the solid, γ_{SL} represents the interfacial tension between the solid surface and liquid phase and γ_L is the surface tension of the liquid (see Fig. 2). Due to the size limitation of the Vitreloy 105 samples (i.e. only 3 mm in diameter), dynamic contact angle measurements could not be performed. Therefore, the static contact angle was taken as the equilibrium contact angle in this study.

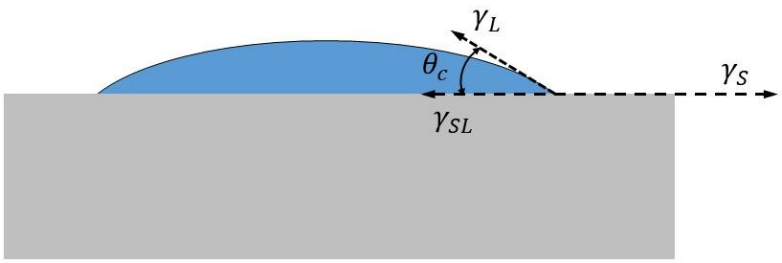

Fig. 2. Schematic diagram for the contact angle of a liquid droplet on a solid surface according to the Young-Dupre's equation

Static contact angle (SCA) values were recorded for the different surface patterns using a contact angle goniometer (DataPhysics OCA100, DataPhysics, Germany) together with a camera-based optical measurement system at a constant temperature of 25℃ and a humidity level around 50%. The shape of a 0.5 µL droplet of a testing liquid deposited on the measured surfaces was captured by the camera once the equilibrium state was reached. The SCA was then determined by analysing the image using a software (SCA20) provided by DataPhysics. The process of placing the liquid droplet on the sample surface is shown in Fig. 3. The contact angle recorded in this study was the average value of the left and right SCA as shown in Fig. 4. Given that it took a very short time to complete one measurement, evaporation was considered to be negligible.

Fig. 3. The process of placing a liquid droplet on a sample surface

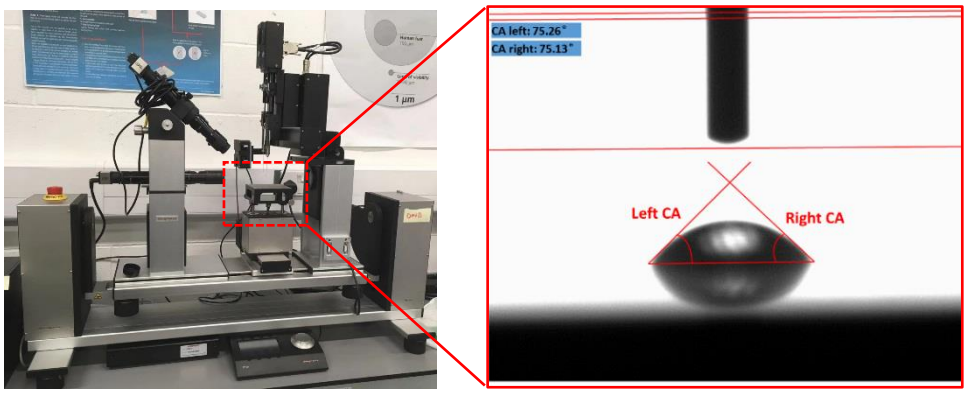

Fig. 4. Contact angle measurement set-up

Satriano et al. (2003) reported that the surface free energy (SFE) also plays an important role in cell attachment and protein adsorption. Therefore, in order to support future studies specifically focussed on cellular behaviour for laser-textured Vitreloy 105 surfaces, the SFE value of all the samples was also assessed. SFE has been widely determined via the Owens-Wendt-Rabel-Kaeble (OWRK) method (Owens and Wendt, 1969). In this method, the SFE of a solid, γ_S^T, is considered to be the sum of its dispersive, γ_S^d, and its polar, γ_S^p , component:

$$\gamma_S^T = \gamma_S^p + \gamma_S^d \tag{3}$$

The following equation is also considered:

$$\gamma_{SL} = \gamma_s + \gamma_L - 2\sqrt{\gamma_S^d \gamma_L^d} - 2\sqrt{\gamma_S^p \gamma_L^p} \tag{4}$$

where γ_L^d and γ_L^p are the dispersive and polar parts of the surface tension for a testing liquid, respectively. γ_{SL}, γ_s and γ_L have already been defined earlier in Equation 2. In combination with the Young-Dupre's equation, a linear equation ($y = mx + c$) can be obtained, as follows:

$$\underbrace{\frac{\gamma_L(1+\cos\theta_c)}{2\sqrt{\gamma_L^d}}}_{y} = \underbrace{\sqrt{\gamma_S^p}}_{m} \cdot \underbrace{\sqrt{\frac{\gamma_L^p}{\gamma_L^d}}}_{x} + \underbrace{\sqrt{\gamma_S^d}}_{c} \tag{5}$$

This means that two testing liquids are needed to calculate the SFE of a solid. Distilled-deionized water (DD water) and ethylene glycol were selected in this study to quantify the SFE of the Vitreloy 105 specimens before and after the laser surface texturing operations. The SFE values for these two testing liquids together with their polar and dispersive components are given in Table 2.

Table 2
Detailed values of the surface free energy for the employed testing liquids.

Liquid	Dispersive energy (γ_L^d) (mN/m)	Polar energy (γ_L^p) (mN/m)	Total surface energy (γ_L^T) (mN/m)
Distilled-deionized water	21.8	51	72.8
Ethylene glycol	29	19	48

The work of adhesion was also assessed in this research. It is defined as the reversible thermodynamic work required to separate the solid-liquid interface from the equilibrium state to an infinite separation distance (Ebnesajjad and Ebnesajjad, 2013). The interfacial attraction increase can result in enhanced work of adhesion. Eq. 6 shows the work of adhesion, W_a, calculation for a liquid-solid combination based on the OWRK equation:

$$W_a = 2\left(\sqrt{\gamma_S^d \gamma_L^d} + \sqrt{\gamma_S^p \gamma_L^p}\right) \tag{6}$$

The definition of the parameters γ_S^d, γ_L^d, γ_S^p, γ_L^p were given earlier.

2.4. Surface analysis

The surface topography of the specimens before and after laser surface texturing was examined by a non-contact three-dimensional surface profiler (S mart Series, Sensofar, Barcelona, Spain) using its confocal operating mode and the associated analysis software (SensoMap). As an extension of the surface profile metric R_a, S_a represents the arithmetical mean height of the whole surface area in the field of view of the optical surface profiler. Therefore, the surface roughness on the amorphous alloy pre and post laser texturing was characterized by S_a. The surface roughness was measured three times and the average value was calculated for each specimen. The surface patterns were also characterized by a field emission scanning electron microscope (1540XB, Carl Zeiss, Germany). This microscope is also equipped with an energy dispersive X-ray (EDX) micro-analyzer (INCA X-sight, Oxford Instruments, UK), which was used for qualitative chemical composition analysis. Additional elemental analysis was carried out with an X-ray photoelectron spectroscopy (XPS) instrument using an ESCALAB^{TM} Xi$^+$ spectrometer microprobe (from Thermo Fisher Scientific, USA) to evaluate chemical composition variations before and after laser surface texturing. The X-ray spectra were acquired using a monochromatic Al Kα X-ray

source. The XPS data were then analysed with the XPS PEAK4.1 software using Shirley backgrounds. Both the survey and narrow scan spectra were recorded from analysed areas 300 × 700 μm^2.

3. Results and discussion

3.1 Surface topography analysis

Nanosecond pulsed laser texturing is a localised thermal machining process in which the laser-induced heat rapidly melts and evaporates the irradiated material. The controlled delivery of successive pulses enables the generation of specific patterns on the surface of workpieces. The dimensions of the laser-fabricated surface structures vary with laser parameters and scanning strategies. This section reports the results obtained when the scanning electron microscope (SEM) and the non-contact three-dimensional surface profiler (using its confocal mode) were employed to characterise the surface topography variation of the Vitreloy 105 metallic glass samples before and after laser texturing.

3.1.1. Effect of the type of laser-fabricated patterns on the surface topography

SEM micrographs and their corresponding 3D surface profiles of the laser textured surfaces are presented in Fig. 5 and Fig. 6 to display the typical topography generated on the surface of the Vitreloy 105 samples for the two types of microscale patterns considered, i.e. dimples and grooves. The patterns presented in these figures were processed with the same laser fluence of 30 J/cm^2. To achieve the dimple pattern shown in Fig. 5, the distance between two adjacent irradiated spots was set at 80 µm as this resulted in the formation of single craters. The average diameter and depth of the single craters were 32.23 µm and 2.44 µm, respectively. It can be observed from Fig. 5 that the surfaces experienced heating, melting, vaporisation as well as material ejection and redeposition as evidenced by the occurrence of re-solidified droplets on the sample. In comparison with the surface roughness of the as-cast specimen, which was S_a = 0.065 µm, the roughness of this dimple textured surface was measured to be S_a = 0.17 µm. The pulse overlap value used to generate the grooves shown in Fig. 6 was 84%, which corresponds to a scanning speed value of 100 mm/s. The track distance was set at 100 µm for this particular example. The average depth and width of these laser-ablated grooves were measured to be about 27.1 µm and 25.1 µm, respectively. Compared to the diameter of craters on the dimple patterned surface, the width of the grooves was reduced slightly but the depth was increased significantly. This is due to the accumulation of single material removal events over a given area as a result of the overlap between two successive laser pulses. When comparing two grooves, a higher overlap means that the amount of cycles of melt ejection for a given distance along the groove is increased. In addition, compared to the dimple pattern, Fig. 6 shows a higher occurrence of fully ejected and re-solidified droplets around the grooves. The roughness of the groove-textured surface was measured to be S_a = 8.51 µm, which was much higher than that of the dimple-textured (0.17 µm) and as-cast samples (0.065 µm), as expected.

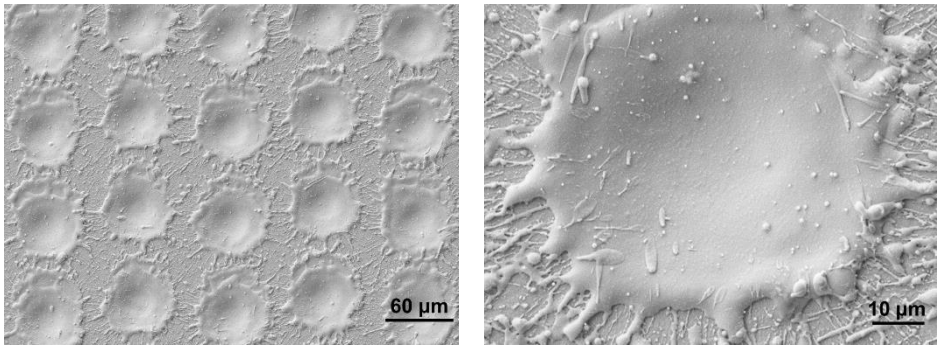

(a) (b)

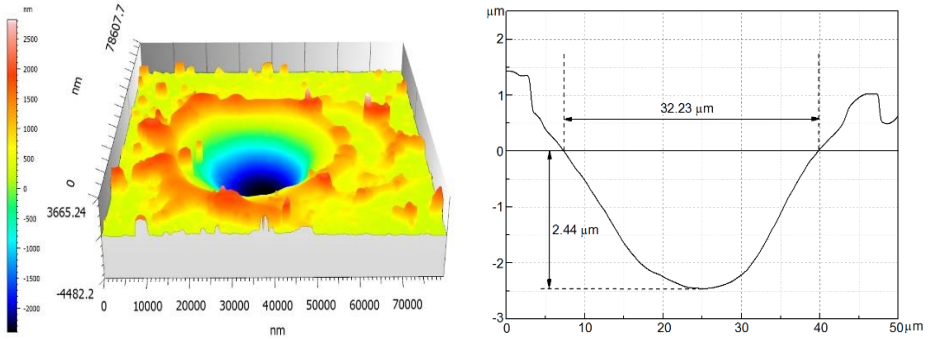

(c) (d)

Fig. 5. Example of a dimple pattern. (a) General view; (b) Enlarged view of (a); (c) 3D profile of a typical dimple; (d) representative cross-section profile of the dimple.

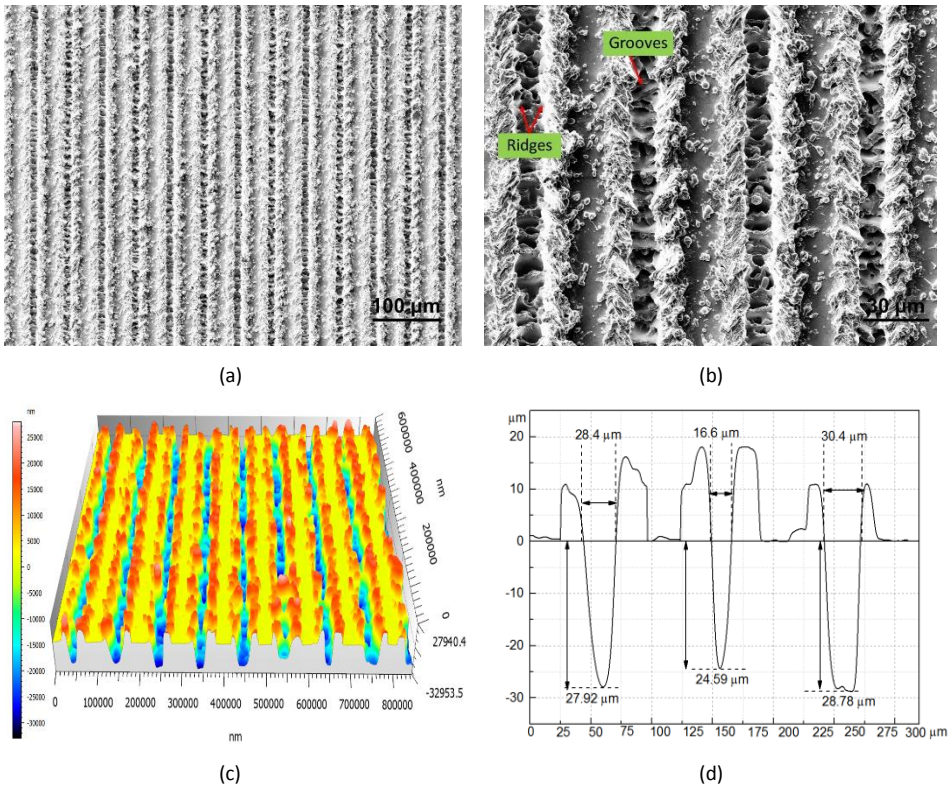

(a) (b)

(c) (d)

Fig. 6. Example of a groove patterns. (a) General view; (b) Enlarged view of (a); (c) 3D profile of the groove structure; (d) Cross-section profile of groove tracks.

3.1.2. Effect of the parameter "distance" on the resulting topography

In the current study, it has to be clarified that the values of the track distance, d_s, and lateral displacement, A, in the case of the dimple patterns were set to be equal and henceforth referred to as "distance". The "distance" values were set to be 60, 70, 80, 90 μm for dimple patterns and 80, 90, 100, 110 μm for groove patterns. Table 3 reports the measured surface roughness, S_a, of all samples. As could be expected, it is observed that the roughness for the groove-textured surfaces decreases with the increase in distance and that this trend is also generally present for the dimpled surfaces.

The SEM images of the dimple-textured and groove-textured specimens treated with the same laser fluence of 30 J/cm^2 and the same scanning speed of 200 mm/s (for the groove patterns) but with different values of the parameter "distance" are shown in Fig. 7 and Fig. 8, respectively. For a small distance on the dimple-textured surface, the craters are located next to each other and there is a very limited area of flat (i.e. unprocessed) surface between two neighbouring craters. With the increase of the distance, such virgin area becomes more visible. The increase in the proportion of such flat area on

the surface results in the natural decrease in the value of S_a. Therefore, such differences in the area not irradiated by the laser drives the surface roughness variation for different values of the parameter "distance". Given the fixed scanning speed associated with the results shown in Table 3, this explanation is also applicable to the surface roughness evolution of the groove-textured samples. In particular, an increase in the parameter "distance" also results in a decrease of the surface roughness for groove-textured samples.

Table 3
Surface roughness of patterned samples with different values for the parameter "distance".

Distance (μm)	S_a (μm)	
	Dimple pattern	Groove pattern
60	0.62 ± 0.06	-
70	0.23 ± 0.05	-
80	0.17 ± 0.03	3.79 ± 0.22
90	0.21 ± 0.06	3.24 ± 0.08
100	-	3.00 ± 0.13
110	-	2.89 ± 0.17
as-cast	0.065 ± 0.01	

Note: the scanning speed used for all groove pattern results presented in this table was 200 mm/s. The errors reported correspond to one standard deviation.

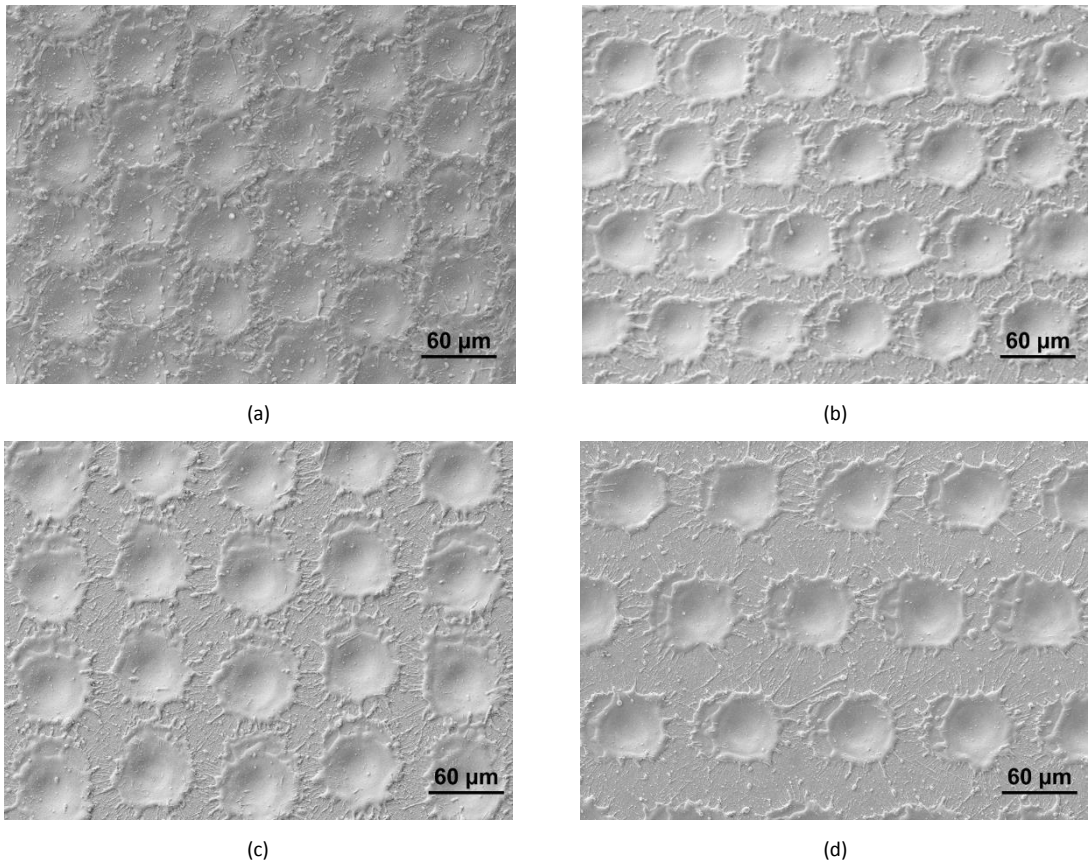

(a) (b)

(c) (d)

Fig. 7. SEM micrographs of dimple-textured surfaces treated with different values of the parameter "distance": (a) 60 μm, (b) 70 μm, (c) 80 μm, (d) 90 μm.

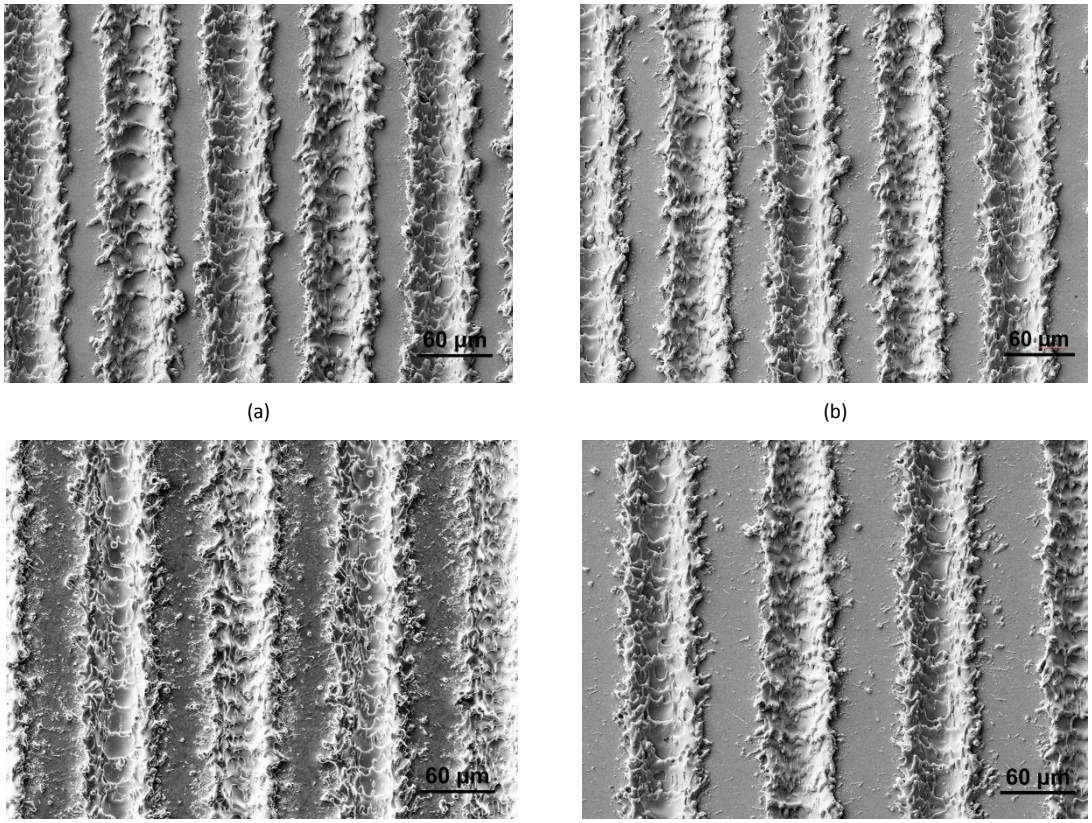

(a) (b)

(c) (d)

Fig. 8. SEM micrographs of groove-textured surfaces treated with different values of the parameter "distance": (a) 80 µm, (b) 90 µm, (c) 100 µm, (d) 110 µm.

3.1.3. Effect of scanning speed on the topography of groove-textured specimens

Fig. 9 displays the SEM micrographs of groove-textured surfaces generated using constant pulse duration, laser fluence and track distance, i.e. 30 J/cm^2, 220 ns, and 100 µm, but for varying scanning speed values of 100, 200 and 300 mm/s in order to change the pulse overlap. From this figure, it can be seen that the scanning speed can change the topography of the grooves significantly. This results from the varying number of delivered pulses per unit length. More specifically, an increased number of pulses per unit length leads to more events of molten material ejection, as is evident from the qualitative observation of the density of re-deposited material around the grooves in Fig. 9. It was reported in our previous work (Jiao et al., 2019) that when the scanning speed increases from 100 mm/s to 300 mm/s, the maximum temperature of the first irradiated site reduced from 2300 K to 1950 K during the delivery second pulse. Consequently, the volume of ejected molten material from the formation of a second melt pool at that particular site is also reduced. In addition, with a lower scanning speed, the bottom of the grooves presents a more distinct hierarchical structure. According to (Huang et al., 2016) this can increase the effective surface area and hence improve the wettability. Further, as shown in the inset of Fig. 9, the average width of the fabricated grooves was measured to be 25.1 µm, 28.6 µm and 26.5 µm, and the depth was 27.1 µm, 10.2 µm and 5.6 µm when the scanning speed varied from 100 to 300 mm/s. Moreover, the surface roughness, S_a, was also greatly decreased from 8.51 µm to 1.91 µm with the increase in scanning speed. The dimensions of the grooves and their corresponding roughness values are summarised in Table 4. Overall, Fig. 9 and Table 4 indicate that laser scanning speed has an important influence on the topography of groove-textured samples. Therefore, selecting a suitable scanning speed value should be critical for fabricating such patterns with a view of achieving optimal wetting property on Vitreloy 105 amorphous alloys.

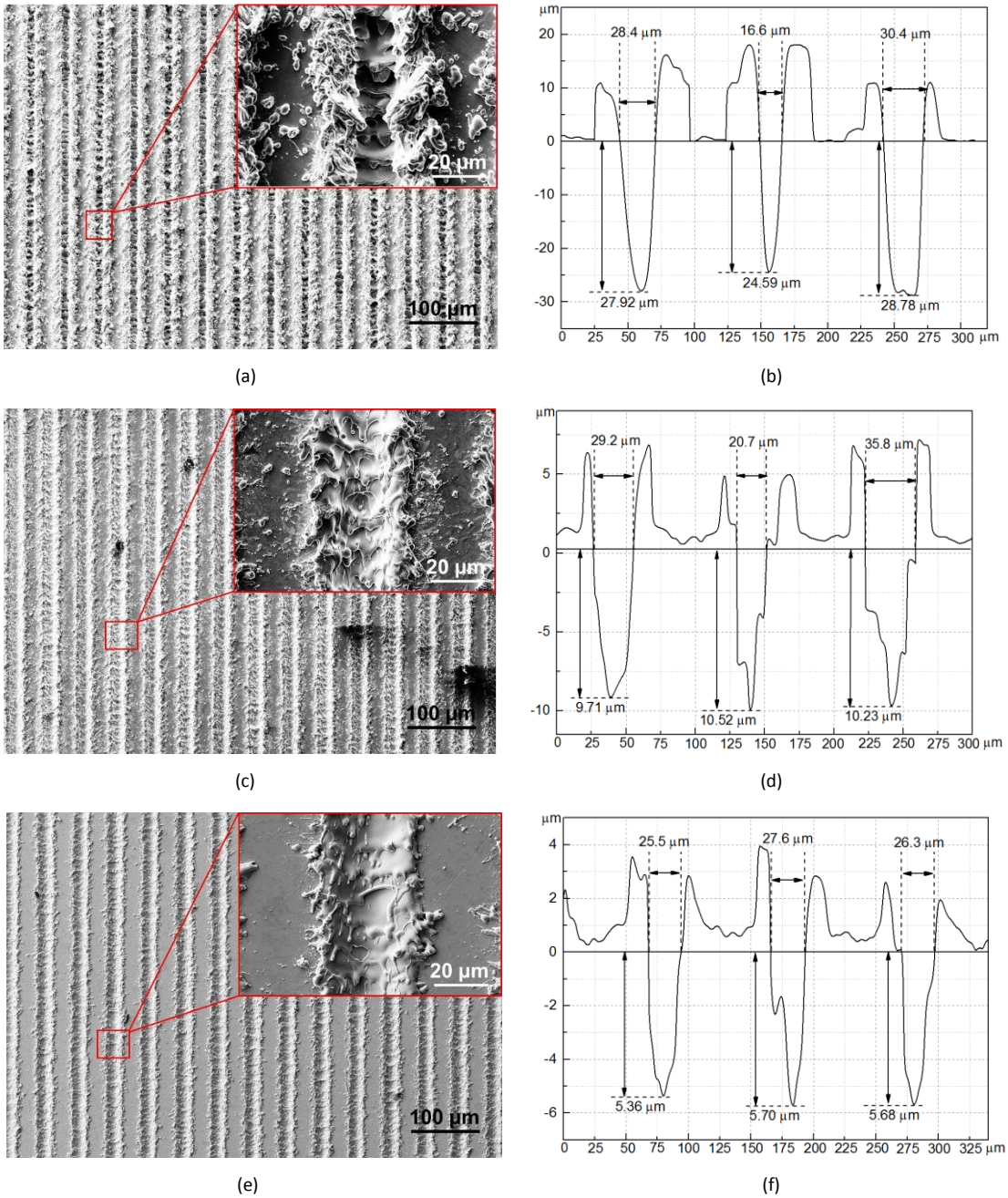

Fig. 9. SEM micrographs of groove-textured surfaces treated with different scanning speed values: (a, b) 100 mm/s, (c, d) 200 mm/s and (e, f) 300 mm/s. Figures (b), (d) and (f) show the associated 3D topography and sectional profile of (a), (c) and (e).

Table 4
Dimensional and roughness data of groove patterns fabricated with various laser scanning speed values.

Laser scanning speed (mm/s)	Groove width (µm)	Groove depth (µm)	Roughness S_a (µm)
100	25.1 ± 3.73	27.1 ± 1.11	8.51 ± 0.51
200	28.6 ± 3.79	10.2 ± 0.21	3.00 ± 0.13
300	26.5 ± 0.53	5.6 ± 0.10	1.91 ± 0.29

Note: the errors reported correspond to one standard deviation.

3.1.4. Effect of laser fluence on the topography of dimple-textured specimens

Laser fluence can significantly affect the dimensions of single craters. Consequently, it is expected that this parameter plays an important role in the resulting surface topography and roughness of the processed samples. Fig. 10 and Table 5 show the SEM micrographs and their corresponding cross-

section profiles, as well as the measured surface data of the dimple-textured specimens. It can be seen from this figure that the density of material re-deposited on the edges of the craters was low and the craters were much shallower under the laser fluence of 10 J/cm^2 in comparison to higher laser fluence conditions. Thus, such fluence value leads to only slight changes in surface topography compared to the as-cast material. This is confirmed quantitatively by the surface roughness data reported in Table 5. A higher laser fluence led to an increased diameter and depth of the machined craters. However, the rate of increase in diameter with laser fluence is not linear and reached a plateau around 30 J/cm^2. This may be attributed to the ablation process mechanism transitioning from melting-dominated to vaporisation-dominated. When the laser fluence reached 50 J/cm^2, Fig. 10(e) shows that a large volume of molten material splashed and re-solidified around the craters. This resulted in a much rougher surface compared to the other two fluence values considered. Thus, for fabricating textured patterns with desired wettability, the laser fluence should be carefully considered as well.

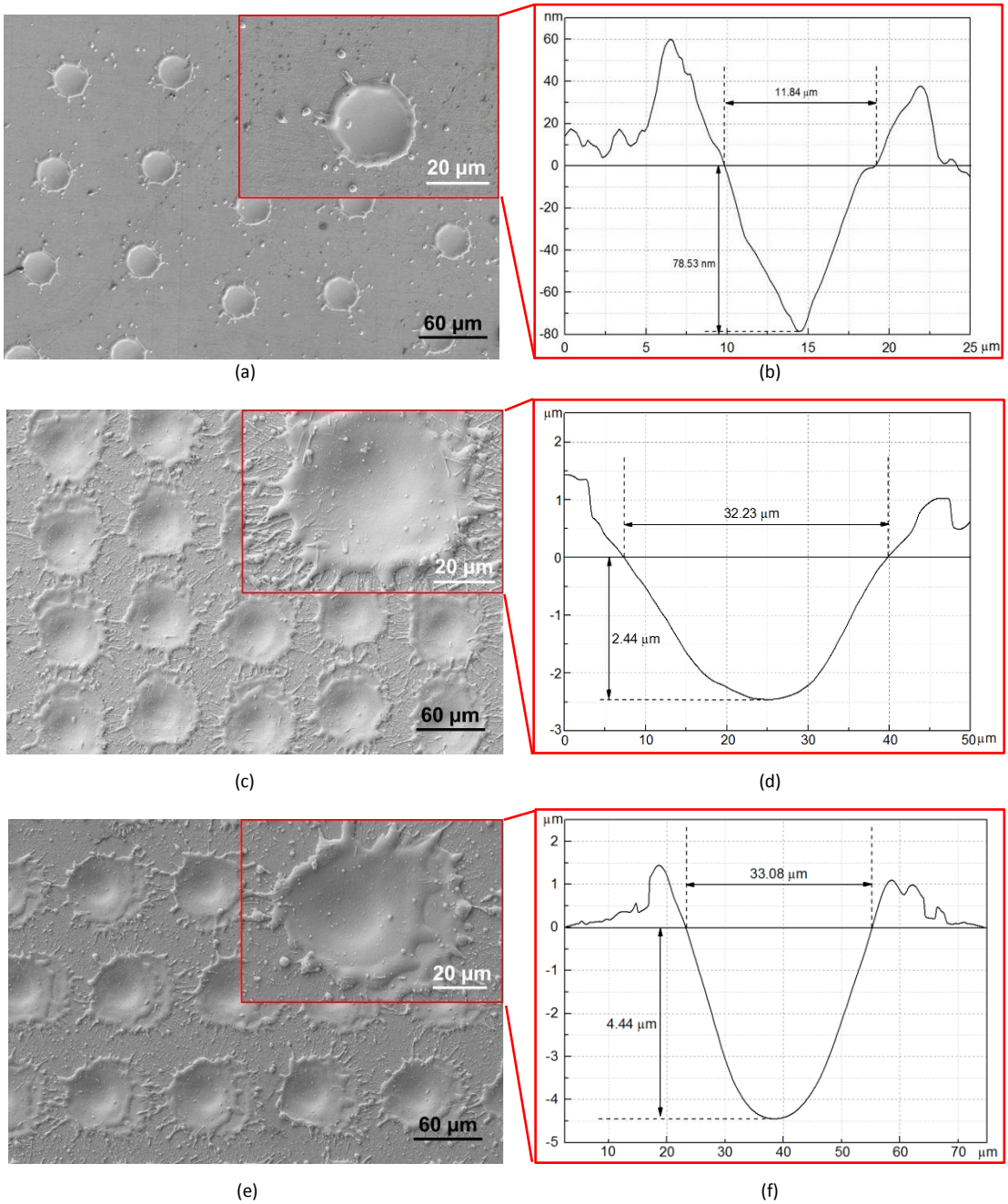

Fig. 10. SEM micrographs of dimple-textured surface treated with various laser fluence of (a) 10 J/cm^2, (c) 30 J/cm^2, (e) 50 J/cm^2 and corresponding cross-section profile for a selected crater (b) (d) (f).

Table 5
Dimensional and roughness data of dimple pattern structures created by various laser fluence values.

Laser fluence (J/cm^2)	Crater diameter (μm)	Crater depth (μm)	Roughness S_a (μm)
10	11.84 ± 0.61	0.08 ± 0.01	0.07 ± 0.02
30	32.23 ± 2.16	2.44 ± 0.41	0.17 ± 0.03
50	33.08 ± 1.99	4.44 ± 0.61	0.41 ± 0.06
As-cast	-	-	0.065 ± 0.01

Note: the errors reported correspond to one standard deviation.

3.2 Analysis of surface wettability

3.2.1 Contact angle measurements

The measured surface contact angle (SCA) values of the Vitreloy 105 BMG samples pre and post laser texturing are presented in Fig. 11. As a reference, the SCAs of the polished sample wetted with the two liquids considered (i.e. DD water and ethylene glycol) are also given (i.e. 35.17° and 19.94°, respectively). These values are smaller than the Berg limit (θ< 65°) (Vogler, 1998), which means that the polished as-cast sample is originally hydrophilic. Following laser irradiation, all surfaces with dimple and groove patterns remained hydrophilic, as evidenced by the measured SCAs values shown in Fig. 11. The measurements also reveal that the SCAs of the samples with the dimple patterns tended to be larger than that of the original as-cast surface, while the SCAs of the specimens textured with the groove patterns were generally smaller than that of the as-cast sample. This implies that the hydrophilicity of the Vitreloy 105 BMG was generally weakened following laser texturing with the dimple structures but generally strengthened with the groove patterns. This observed enhanced hydrophilicity of the groove-textured samples is consistent with their significantly higher surface roughness. This result is also in-line with other reports in the literature in which laser surface texturing of metallic specimens was also studied, such as in (Pfleging et al., 2015). However, compared to the as-cast sample, a weakened hydrophilicity is observed on the dimple-patterned surfaces despite their higher surface roughness. Thus, while one may see the influence of the type of patterns on wettability, as expected from the literature discussed earlier, it is not possible to consider the variation of the surface roughness alone to draw definitive conclusions about the evolution of the hydrophilicity of a surface.

Fig. 11(a) and (b) depict the SCA values for the samples wetted by both testing liquids, DD water and ethylene glycol, as a function of the parameter “distance”. Unlike the evolution of the surface roughness as a function of this parameter, there is no specific trend for the change in SCA value with the increase in “distance” for the two types of surface patterns. In addition, the SCA evolution of the dimple-textured surfaces treated with different laser fluence values is shown in Fig. 11(c). This particular plot reveals that the SCA decreases with the increase of the fluence when the surface was wetted by both liquids. This indicates that a higher laser fluence could enhance the hydrophilicity of the dimple-textured surface. Nevertheless, the SCA values for this type of surface texture were still found to be higher than that of the as-cast sample for the large majority of the tested conditions. Fig. 11(d) presents the SCA measurements for the groove patterns as a function of the scanning speed. In this case, it is observed that a slower scanning speed can enhance the hydrophilicity of this surface texture.

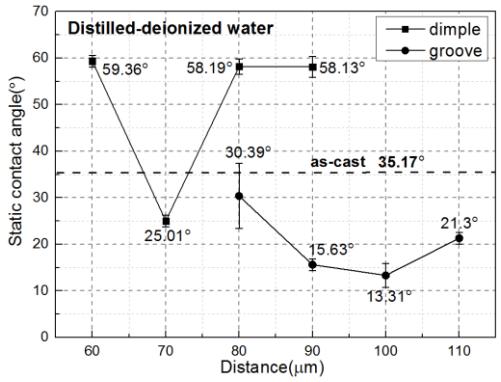

(a)

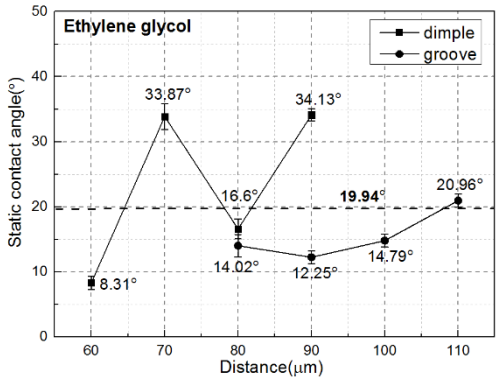

(b)

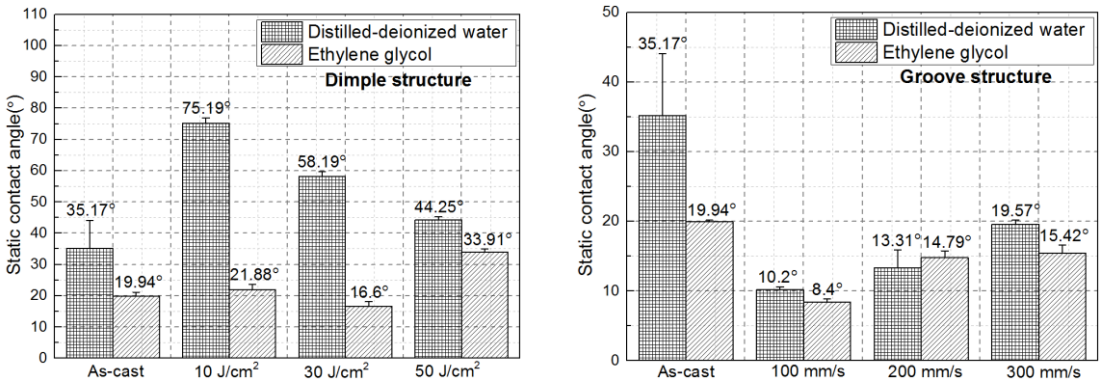

Fig. 11. Surface contact angle measurements before and after laser surface texturing; (a) data obtained with DD water as the testing liquid and (b) with ethylene glycol on specimens treated with different values of the parameter "distance"; (c) data obtained with DD water and ethylene glycol on the dimple-textured samples treated with different fluence values (d) DD water and ethylene glycol results on the groove-textured samples treated with different scanning speeds.

Representative images of the water contact angle measurements obtained with different surface patterns and processed by different laser parameters are also provided in Fig. 12. According to the Wenzel model (Wenzel, 1936), the wetting behaviour of a surface can be enhanced with increased roughness as the contact angle θ_w obeys the following equation:

$$\cos\theta_w = r\cos\theta \tag{7}$$

where r is the surface roughness; θ is the surface contact angle for the original, as-cast sample, which corresponds to the initial surface properties of the target material.

Eq. (7) infers that when an original surface is hydrophilic, it can become more hydrophilic by increasing its roughness, while an initially hydrophobic surface evolves as more hydrophobic with a higher roughness. The analysis reported earlier in section 3.1 showed that the roughness of all groove-textured surfaces was larger than that of the dimple-textured and as-cast samples. Besides, since the as-cast polished Vitreloy 105 surface was originally hydrophilic, the Wenzel model can be used to explain why the processed surface becomes more hydrophilic when texturing groove patterns. However, as mentioned earlier, for the dimple patterns, the surface roughness of all the samples was also higher than that of the as-cast specimen. However, the hydrophilicity was still reduced after laser texturing. In this case, the Wenzel model cannot explain this observation. As discussed earlier, surface topography is not the only factor that affect surface wettability. Indeed, surface chemistry also plays an important role in the wettability evolution. Thus, the influence of the surface chemical composition changes induced by laser processing may be a likely reason to explain why the dimple structures resulted in a weakened hydrophilicity despite the increased roughness from that of the as-case sample. Therefore, the underlying mechanism of wettability modification for the laser textured Zr-based amorphous alloy will be discussed from a surface chemistry perspective later in section 3.3.

Finally, it can also be said that the surface contact angle measurement results presented here are consistent with those of Pfleging et al. (2015), who laser textured dimple and groove patterns to modify the surface wettability of Ti-6Al-4V substrates. In particular, these authors observed that groove patterns could significantly increase the hydrophilicity of the processed surface. From the results presented here, it is also clear that the generation of a groove-textured surface is a suitable approach for enhancing the hydrophilicity of Vitreloy 105.

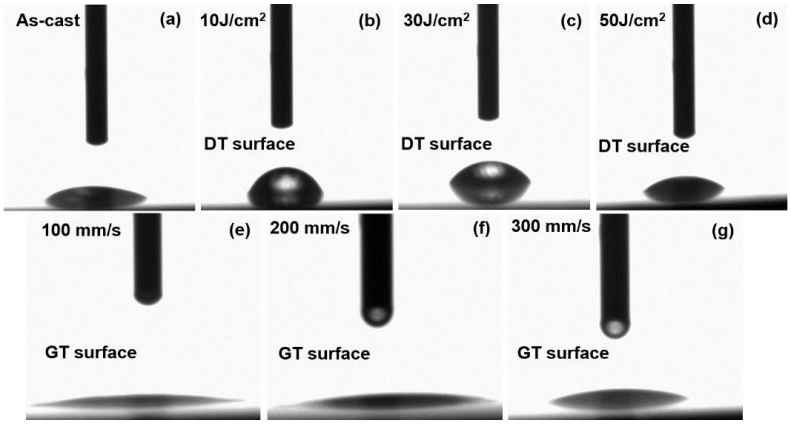

Fig. 12. Representative images recorded during water contact angle measurements on Vitreloy 105 processed with different surface patterns and laser parameters: (a) as-cast; (b) DT surface with 10 J/cm^2; (c) DT surface with 30 J/cm^2; (d) DT surface with 50 J/cm^2; (e) GT surface with 100 mm/s; (f) GT surface with 200 mm/s; (g) GT surface with 300 mm/s. Note: "DT" means dimple texture and "GT" groove texture.

3.2.2 Surface free energy

In this section, the obtained surface free energy (SFE) data are explored as a function of the textured pattern. It has to be mentioned that the effect of the parameter "distance" on the SFE and work of adhesion of the Vitreloy 105 samples is not presented due to the fact that no specific dependence had been observed earlier between this parameter and the contact angle (c.f. Fig 11(a) and Fig. 11(b)). Fig. 13 shows the total SFE together with the polar and dispersive components data obtained for the as-cast and laser-textured Vitreloy 105 samples. It can be seen from this figure that the total SFE of these laser-textured samples is comprised in a relatively large range of values, from 46.07 to 125.74 mN/m, around that of the as-cast specimen (81.04 mN/m). A more detailed observation reveals that the total SFE of the dimple-textured samples is always lower than that of the as-cast specimens, although it is noted that this is marginally true in the case of the smallest fluence value considered. For the surfaces with the groove patterns, the total SFE is always clearly higher than that of the as-cast specimen. Moreover, the polar component of the SFE is consistently the much higher contributor for the groove-textured samples, while it is the dispersive component of the SFE, which is the more significant contributor for the dimple-textured specimens. Unlike the monotonous relationship of the SCA with the laser fluence or scanning speed, there is no linear trend between surface free energy and these two parameters in the processing window considered here.

Among others, it was reported by Sarapirom et al. (2013) that polar molecules, which can be characterised by the polar component of SFE, play a positive role in the enhancement of wettability. In combination with the contact angle measurements reported in the previous section (section 3.2.1), it can be said that the high polar surface energy of the specimens with groove patterns contributes to the enhanced hydrophilicity.

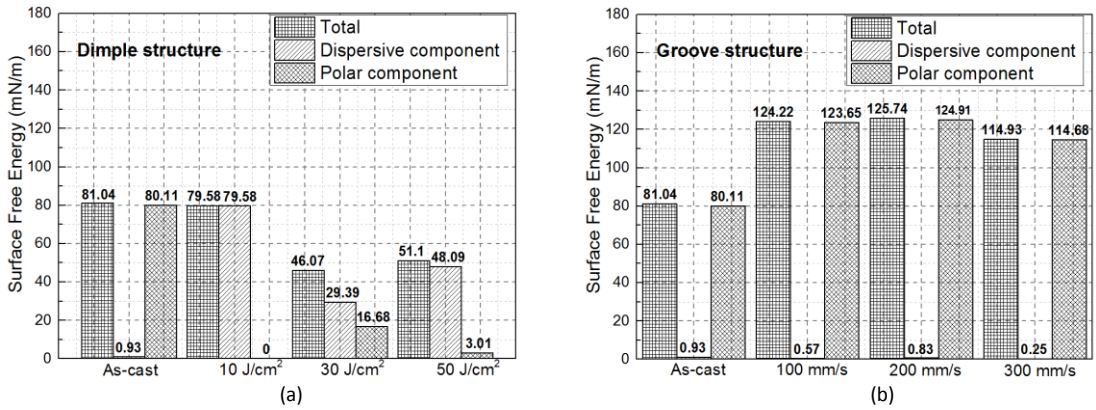

Fig. 13. Surface free energy as well as dispersive and polar components data obtained for the as-cast and laser textured Vitreloy 105 specimens.

3.2.3 Work of adhesion

Work of adhesion results for the as-cast and laser textured Vitreloy 105 specimens wetted by both liquids (DD water and ethylene glycol) are shown in Fig. 14. The work of adhesion for the as-cast specimen was 136.84 and 88.41 mN/m when wetted by DD water and ethylene glycol, respectively. It should be noted that the work of adhesion for the samples textured with groove patterns is always higher than that of the as-cast specimens for both liquids. In contrast, the work of adhesion for the surfaces textured with dimple patterns is lower than the as-cast ones, for the DD water while it is either equal or only slightly higher for the ethylene glycol. These results are generally consistent with the surface free energy calculations and surface contact angle measurements. However, no particular trend can be identified between the work of adhesion and the scanning speed for the groove patterns or with the laser fluence for the dimple-patterned surfaces.

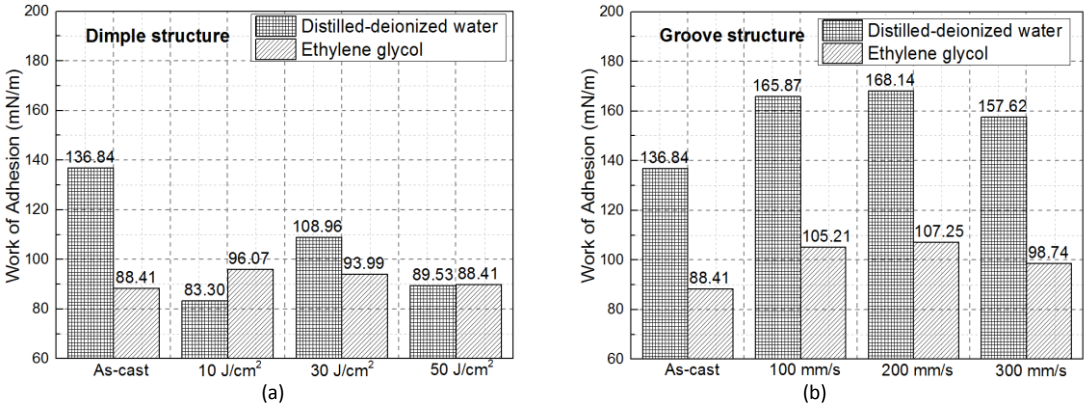

Fig. 14. Work of adhesion for as-cast and laser textured surfaces with dimple and groove patterns.

3.3 Surface chemistry

As pointed out by Fasasi et al. (2009), for instance, the surface chemical composition of a metallic substrate can be modified by laser texturing mainly through material vaporisation and chemical reaction with the atmosphere, principally oxidation. To explore variations in the chemical composition on the surface of the BMG samples and to further correlate surface chemistry with wettability, the specimens were analysed using energy dispersive X-ray detector (EDX) mapping and X-ray photoelectron spectroscopy (XPS). The dimple-textured and groove-textured BMG samples considered for the surface chemistry analysis were treated with the same laser fluence of 30 J/cm^2 and also the same parameter “distance” of 90 µm. In addition, the scanning speed for the groove-textured sample was set at 200 mm/s. The EDX data obtained to assess the distribution of Zr, Cu, Ni, Al, O, and C for the as-cast, dimple, and groove-textured specimens are shown in Fig. 15. Given that the content of Ti is the lowest among all the elements contained in the composition of Vitreloy 105, its presence was difficult to detect and thus, data for Ti are not presented here. From this figure, it can be clearly seen that the Zr, Cu, Ni, Al, O, and C elements are uniformly distributed on the as-cast specimen. For the dimple-textured sample, the elements Ni, Al, C, and O are uniformly distributed on the irradiated surfaces, while some small areas corresponding to the rims of the single craters may suggest a reduction of the Zr and Cu elements distribution. However, this outcome may be an artefact resulting from the topography of the laser-induced protrusions. This observation is also applicable to the elemental distribution of the groove-patterned samples as the locations of such black areas show a good match with the protrusions of the grooves. Given that EDX mapping is mainly a qualitative analysis technique and that it could not provide specific conclusions about the evolution of the surface chemistry following laser processing, the elemental analysis technique XPS was also employed to investigate chemical changes on the surface of the laser textured BMG samples.

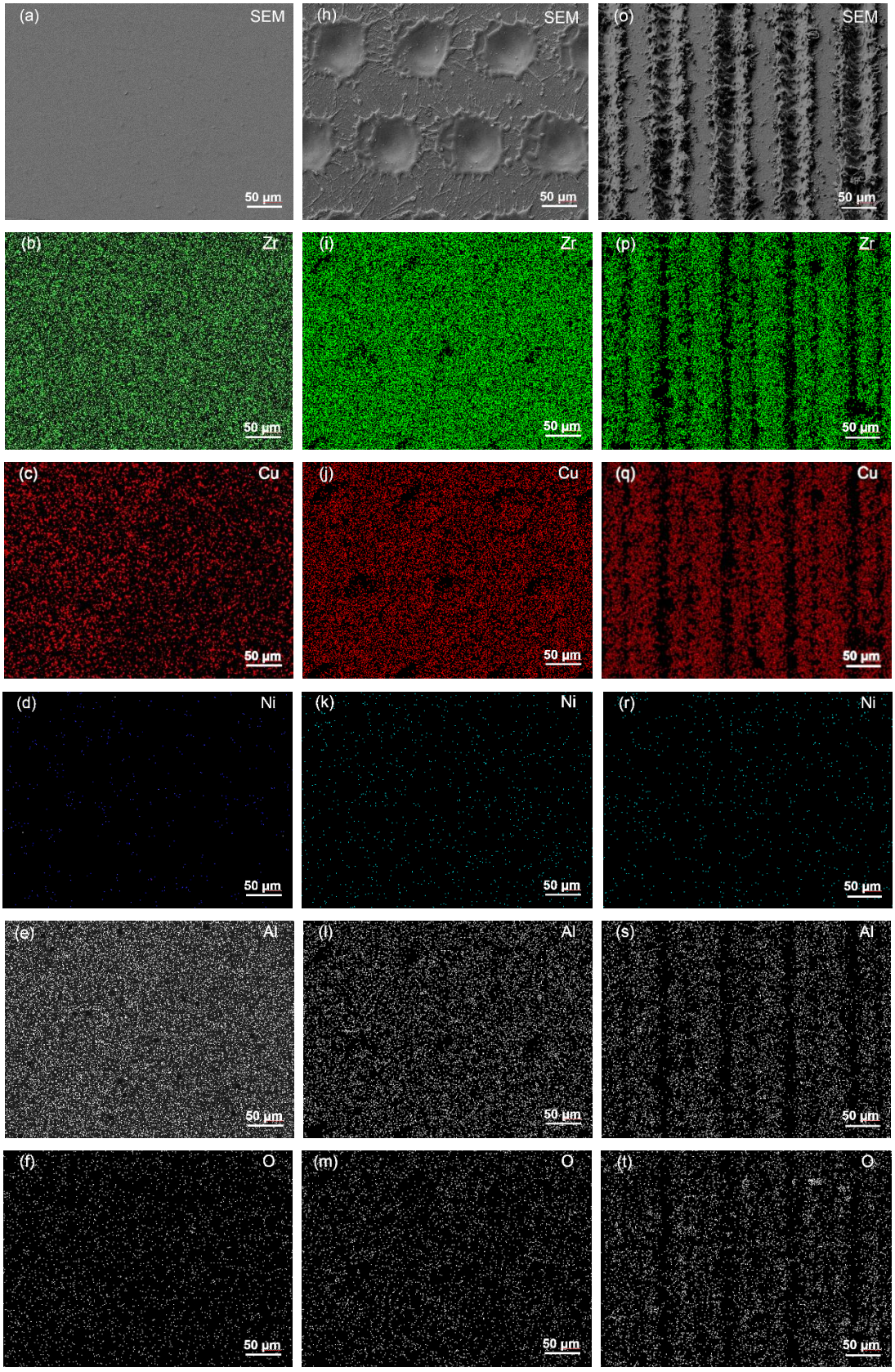
(a)
SEM
50 μm
(h)
SEM
50 μm
(o)
SEM
50 μm
(b)
Zr
50 μm
(i)
Zr
50 μm
(p)
Zr
50 μm
(c)
Cu
50 μm
(j)
Cu
50 μm
(q)
Cu
50 μm
(d)
Ni
50 μm
(k)
Ni
50 μm
(r)
Ni
50 μm
(e)
Al
50 μm
(l)
Al
50 μm
(s)
Al
50 μm
(f)
O
50 μm
(m)
O
50 μm
(t)
O
50 μm

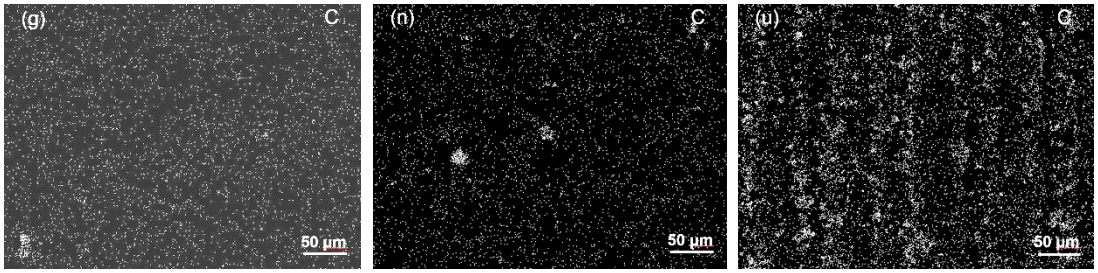

Fig. 15. SEM/EDX element mapping of as-cast (a-g), dimple-textured (h-n) and groove-textured (o-u) laser irradiated surfaces. (a), (h) and (o) are SEM images depicting the corresponding analysed regions; (b-u) are the EDX maps showing the qualitative elemental distributions of Zr, Cu, Ni, Al, O, and C.

The XPS full spectra of all the samples considered for surface chemistry analysis (as-cast, dimple-textured and groove-textured specimens) and the corresponding atomic percentage of the different elements are shown in Fig. 16. It can be seen from the XPS full spectra of the as-cast sample (Fig. 16(a)) that carbon (58.89 %) and oxygen (28.58 %) were detected as the main elements, which is ascribed to surface contamination and oxidation. In addition, some small peaks on the Al 2*p* and Zr 3*d* region were also observed on the as-cast sample surface. This non-laser processed surface also contained negligible amounts of Ti, Cu and Ni elements.

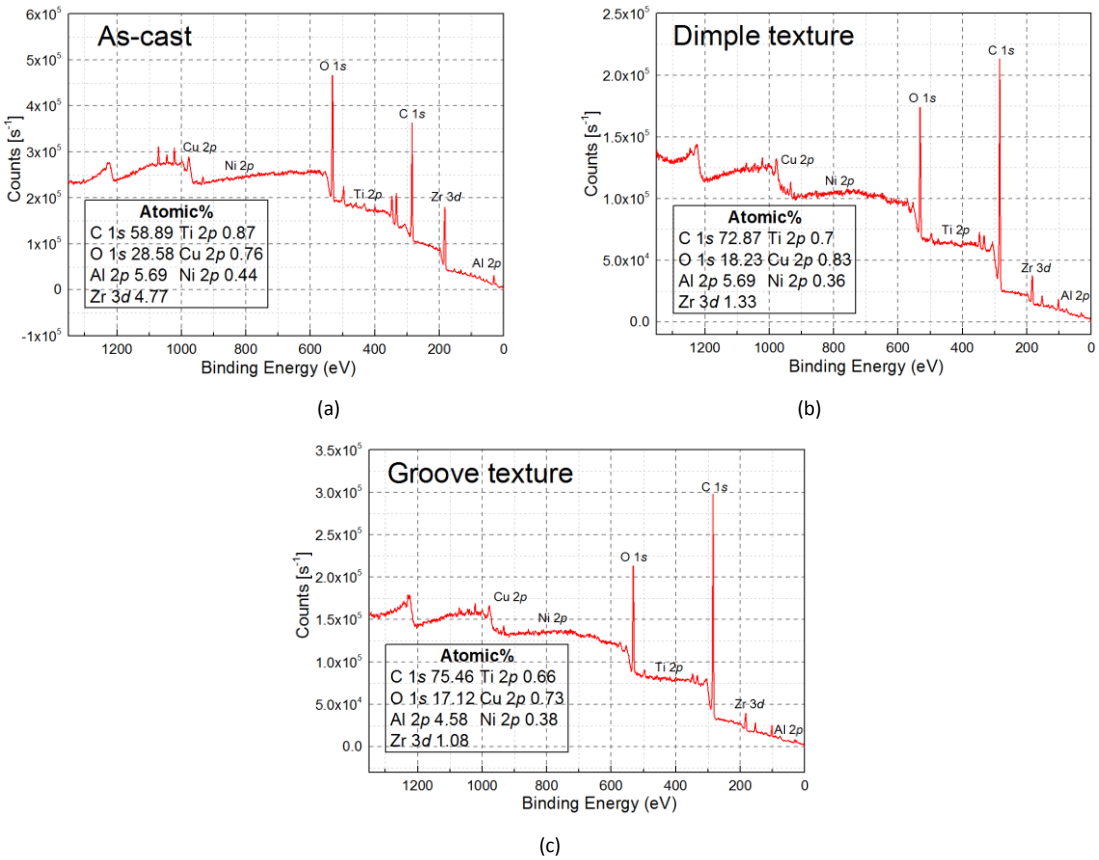

Fig. 16. XPS full spectra of Vitreloy 105 metallic glass samples before and after laser surface texturing: (a) as-cast; (b) dimple-textured specimen; (c) groove-textured specimen.

The detailed atomic elemental composition of the Vitreloy 105 samples without and with textured patterns is shown with the inset of the corresponding XPS spectra in Fig. 16. These data indicate a decrease in the percentage of Zr concentration on the Vitreloy 105 surfaces after laser texturing compared to the as-cast one, which may be attributed to material vaporisation during laser irradiation. In comparison, the Al content remained relatively stable. Furthermore, while the as-cast specimen exhibited a carbon content of 58.89 %, this was increased to 72.87 % and 75.46 % after laser processing for the dimple and groove-textured surfaces, respectively. This implies that more hydrocarbons were

introduced on the sample surface following the laser surface texturing process. In contrast, the oxygen content decreased from 28.58 % for the as-cast specimen to 18.23 % and 17.12 % for the dimple and groove-textured surfaces, respectively, suggesting the removal of metal oxide from the surface. Additionally, due to oxidation and contamination, all samples exhibited a rather low concentration of Ti, Cu, and Ni on their surfaces. When reviewing the related literature earlier, it was reported that carbon groups on the surface should have a significant influence on wettability. Therefore, a higher resolution XPS spectra of carbon was also performed. These are shown in Fig. 17 for the C 1*s* regions. From this figure, three chemical groups of carbon-carbon (C-C) bonds or hydrocarbons species (C-H), as well as carbonyl bonds (C=O) and carboxyl species (O=C-O) were observed on the as-cast sample at the locations of 284.8 eV, 288.6 eV and 292.8 eV, respectively. After laser surface texturing, the intensity of the C-C/C-H peak was reduced, especially for the dimple-textured surface. Based on Huerta-Murillo et al. (2019), this could be attributed to the removal of surface contaminants caused by the laser ablation. Additionally, the intensity of the C=O component was also reduced, again more significantly for the dimple pattern, while the intensity of the O=C-O component was reduced to a non-detectable level for both types of patterns. As pointed out earlier based on literature reports, carbonyl bonds (C=O) and O=C-O species are associated with a hydrophilic behaviour, whereas C-C/C-H bonds increase hydrophobicity.

Based on the reported data, we can reasonably infer that the evolution of the wettability for the two types of laser textured surfaces considered in this study, i.e. dimple-textured and groove-textured, results from the combined effects of laser-induced surface roughness and chemical modifications. More specifically, for the as-cast samples, given that the surface roughness is only 0.065 µm, its contribution to the initial hydrophilicity may be neglected. In this case, the hydrophilic property of the as-cast sample should mainly result from the presence of polar carbonyl bonds (C=O) and carboxyl species (O=C-O). For the dimple-textured sample, the surface roughness was measured to be 0.21 µm. Considering that this value is higher than that of the as-cast specimen, based on the Wenzel model, it could be expected that the hydrophilicity may be enhanced. However, given that the opposite was observed, i.e. a weakened hydrophilicity for the dimple patterns, it can be said that the influence of the surface roughness modification should play a relatively less important role as contributor to the evolution of the wettability compared to the influence of surface chemistry variations. In fact, after laser dimple texturing, the intensity of the hydrophilic carbonyl bonds (C=O) and carboxyl species (O=C-O) were significantly reduced as observed in Fig. 17. The intensity of the hydrophobic C-C/C-H bonds was also reduced. For this reason, it is proposed that the likelihood explanation for the weakened hydrophilicity of the dimple-textured samples is the significantly reduced content of the hydrophilic (C=O) and (O=C-O) bonds. Finally, in the case of the groove-textured sample, the surface roughness was measured to be 3.24 µm. This is 50 times higher than that of the as-cast samples. Thus, although the hydrophilic carbonyl bonds (C=O) and carboxyl species (O=C-O) were reduced after laser texturing, in this case, it is the much higher surface roughness that should be the dominant factor in the hydrophilicity enhancement of the groove-textured samples.

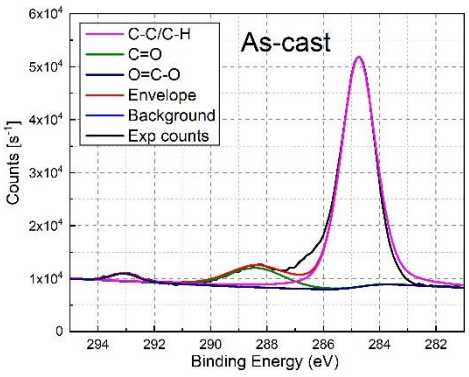

(a)

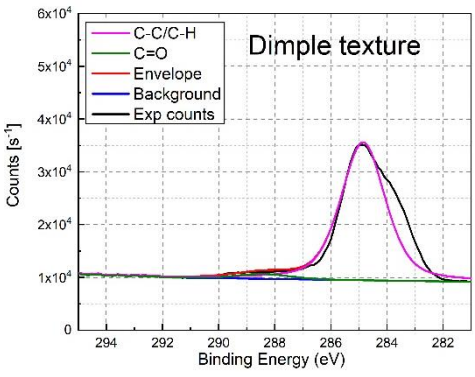

(b)

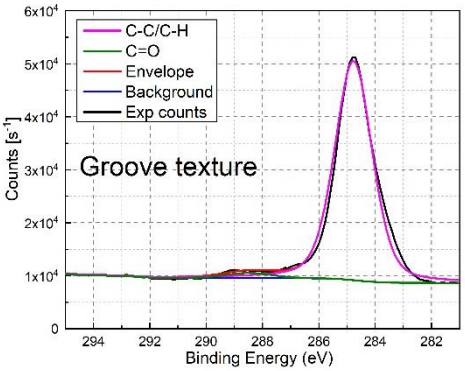

(c)

Fig. 17. High-resolution spectra from the C1s regions on the Vitreloy 105 metallic glass with and without laser surface texturing: (a) as-cast; (b) dimple-textured surface; (c) groove-textured surface.

4. Conclusions

Nanosecond pulsed laser surface texturing was employed to fabricate two types of surface patterns, i.e. dimples and grooves, on a Zr-based metallic glass, also known as Vitreloy 105. These surface patterns were fabricated with the aim to investigate whether they could improve the surface wettability of the as-cast Vitreloy 105 material and hence, enhance the potential of this particular BMG alloy to be considered for biomedical applications. The surface topography and roughness of samples irradiated with different parameters when producing the considered textures were studied and compared. The static contact angle was measured, and the surface free energy was assessed for all samples. Comparisons of surface chemical composition before and after laser texturing were also made via EDX mapping and XPS analysis in an attempt to explain how such laser-induced variations could contribute to the modification of the wettability.

The obtained results confirm the existing literature that surface wettability can be modified intentionally by laser texturing depending of the generated surface patterns and selected process parameters. In line with former reports where laser texturing was applied to other types of metallic materials, it was found that the hydrophilicity of the as-cast Vitreloy 105 surface could be enhanced by texturing groove patterns. Importantly, based on the outcome of the surface topography and chemistry analyses, this increased hydrophilicity could be attributed to the dominant role that a much higher roughness plays for such patterns. In contrast, the hydrophilicity of the as-cast surface was generally deteriorated with the laser texturing of dimple patterns. This result was attributed to the more dominant role that surface chemistry modification plays in this case, and in particular, to the reduction of the hydrophilic carbonyl bonds (C=O) and carboxyl species (O=C-O). Another important outcome of the work presented is that it indicates the possible potential of Vitreloy 105 to be employed in applications for orthopaedic implants when used in combination with laser surface texturing to generate groove patterns on the implant surface. Further complementary investigations on cell viability and attachment by in vitro cell culture on such patterns are currently conducted by the authors.

Acknowledgments

The authors would like to thank Mrs. Jiamei Liu from the Instrumental Analysis Center of Xi'an Jiaotong University for her assistance in the XPS measurement; Dr. David Waugh from Coventry University for his help of contact angle measurement. The lead author (Yang Jiao) acknowledges the financial support from Cardiff University, UK and Xi'an Jiaotong University, China. Emmanuel Brousseau also gratefully acknowledges the financial support provided by the Welsh Government and Higher Education Funding Council for Wales through the Sêr Cymru National Research Network in Advanced Engineering and Materials.

References

Bian, Z., Chen, G., He, G., Hui, X., 2001. Microstructure and ductile–brittle transition of as-cast Zr-based bulk glass alloys under compressive testing. Materials Science and Engineering: A 316, 135-144.

Bizi-Bandoki, P., Valette, S., Audouard, E., Benayoun, S., 2013. Time dependency of the hydrophilicity and hydrophobicity of metallic alloys subjected to femtosecond laser irradiations. Applied Surface Science 273, 399-407.

Ebnesajjad, S., Ebnesajjad, C., 2013. Surface treatment of materials for adhesive bonding. William Andrew.

Fasasi, A.Y., Mwenifumbo, S., Rahbar, N., Chen, J., Li, M., Beye, A.C., Arnold, C.B., Soboyejo, W.O., 2009. Nano-second UV laser processed micro-grooves on Ti6Al4V for biomedical applications. Materials Science and Engineering: C 29, 5-13.

Huang, H., Jun, N., Jiang, M., Ryoko, M., Yan, J., 2016. Nanosecond pulsed laser irradiation induced hierarchical micro/nanostructures on Zr-based metallic glass substrate. Materials & Design 109, 153-161.

Huang, H., Yan, J., 2017a. Investigating shear band interaction in metallic glasses by adjacent nanoindentation. Materials Science and Engineering: A 704, 375-385.

Huang, H., Yan, J., 2017b. Surface patterning of Zr-based metallic glass by laser irradiation induced selective thermoplastic extrusion in nitrogen gas. Journal of Micromechanics and Microengineering 27, 075007.

Huang, L., Cao, Z., Meyer, H.M., Liaw, P.K., Garlea, E., Dunlap, J.R., Zhang, T., He, W., 2011. Responses of bone-forming cells on pre-immersed Zr-based bulk metallic glasses: Effects of composition and roughness. Acta Biomater 7, 395-405.

Huerta-Murillo, D., García-Girón, A., Romano, J., Cardoso, J., Cordovilla, F., Walker, M., Dimov, S., Ocaña, J., 2019. Wettability modification of laser-fabricated hierarchical surface structures in Ti-6Al-4V titanium alloy. Applied Surface Science 463, 838-846.

Jiao, Y., Brousseau, E., Han, Q., Zhu, H., Bigot, S., 2019. Investigations in nanosecond laser micromachining on the Zr52. 8Cu17. 6Ni14. 8Al9. 9Ti4. 9 bulk metallic glass: experimental and theoretical study. Journal of Materials Processing Technology 273.

Kietzig, A.-M., Hatzikiriakos, S.G., Englezos, P., 2009. Patterned superhydrophobic metallic surfaces. Langmuir 25, 4821-4827.

Kumari, R., Scharnweber, T., Pfleging, W., Besser, H., Majumdar, J.D., 2015. Laser surface textured titanium alloy (Ti–6Al–4V) – Part II – Studies on bio-compatibility. Applied Surface Science 357, 750-758.

Li, B.-j., Li, H., Huang, L.-j., Ren, N.-f., Kong, X., 2016. Femtosecond pulsed laser textured titanium surfaces with stable superhydrophilicity and superhydrophobicity. Applied Surface Science 389, 585-593.

Li, H.F., Zheng, Y.F., 2016. Recent advances in bulk metallic glasses for biomedical applications. Acta Biomater 36, 1-20.

Liaw, P.K., Miller, M.K., 2008. Bulk Metallic Glasses. Springer.

Löffler, J.F., 2003. Bulk metallic glasses. Intermetallics 11, 529-540.

Naleway, S.E., Greene, R.B., Gludovatz, B., Dave, N.K., Ritchie, R.O., Kruzic, J.J., 2013. A highly fatigue-resistant Zr-based bulk metallic glass. Metallurgical and Materials Transactions A 44, 5688-5693.

Owens, D.K., Wendt, R., 1969. Estimation of the surface free energy of polymers. Journal of applied polymer science 13, 1741-1747.

Pfleging, W., Kumari, R., Besser, H., Scharnweber, T., Majumdar, J.D., 2015. Laser surface textured titanium alloy (Ti–6Al–4V): Part 1 – Surface characterization. Applied Surface Science 355, 104-111.

Ponsonnet, L., Reybier, K., Jaffrezic, N., Comte, V., Lagneau, C., Lissac, M., Martelet, C., 2003. Relationship between surface properties (roughness, wettability) of titanium and titanium alloys and cell behaviour. Materials Science and Engineering: C 23, 551-560.
Sarapirom, S., Lee, J., Jin, S., Song, D., Yu, L., Han, J., Chaiwong, C., 2013. Wettability effect of PECVD-SiOx films on poly (lactic acid) induced by oxygen plasma on protein adsorption and cell attachment, Journal of Physics: Conference Series. IOP Publishing, p. 012042.
Satriano, C., Carnazza, S., Guglielmino, S., Marletta, G., 2003. Surface free energy and cell attachment onto ion-beam irradiated polymer surfaces. Nuclear Instruments and Methods in Physics Research Section B: Beam Interactions with Materials and Atoms 208, 287-293.
Telford, M., 2004. The case for bulk metallic glass. Materials today 7, 36-43.
Vogler, E.A., 1998. Structure and reactivity of water at biomaterial surfaces. Advances in colloid and interface science 74, 69-117.
Wenzel, R.N., 1936. Resistance of solid surfaces to wetting by water. Industrial & Engineering Chemistry 28, 988-994.